Conformal In-Context Reverse Classification Accuracy: Efficient Estimation of Segmentation Quality with Statistical Guarantees

Matias Cosarinsky, Ramiro Billot, Lucas Mansilla, Gabriel Jimenez, Nicolas Gaggion, Guanghui Fu, Tom Tirer, and Enzo Ferrante

Abstract—Assessing the quality of automatic image segmentation is crucial in clinical practice, but often very challenging due to the limited availability of ground truth annotations. Reverse Classification Accuracy (RCA) is an approach that estimates the quality of new predictions on unseen samples by training a segmenter on those predictions, and then evaluating it against existing annotated images. In this work, we introduce Conformal In-Context RCA, a novel method for automatically estimating segmentation quality with statistical guarantees in the absence of ground-truth annotations, which consists of two main innovations. First, In-Context RCA, which leverages recent incontext learning models for image segmentation and incorporates retrieval-augmentation techniques to select the most relevant reference images. This approach enables efficient quality estimation with minimal reference data while avoiding the need of training additional models. Second, we introduce Conformal RCA, which extends both the original RCA framework and In-Context RCA to go beyond point estimation. Using tools from split conformal prediction, Conformal RCA produces prediction intervals for segmentation quality providing statistical guarantees that the true score lies within the estimated interval with a user-specified probability. Validated across 10 different medical imaging tasks in various organs and modalities, our methods demonstrate robust performance and computational efficiency, offering a promising solution for automated quality control in clinical workflows, where fast and reliable segmentation assessment is essential. The code is available at https://github.com/mcosarinsky/Conformal-In-Context-RCA.

Index Terms—Segmentation quality control, reverse classification accuracy, in-context learning, conformal prediction, uncertainty quantification

I. INTRODUCTION

MAGE segmentation plays a crucial role in many medical practices, particularly for treatment planning, clinical decision making and monitoring disease progression. In these scenarios, evaluating the performance of segmentation methods becomes of utmost importance. Typically, the evaluation is performed on annotated databases using metrics that measure the agreement between predicted segmentations and *ground*

Matias Cosarinsky, Nicolas Gaggion, and Enzo Ferrante are with the Universidad de Buenos Aires, Buenos Aires, Argentina (emails: mcosarinsky@dc.uba.ar, ngaggion@sinc.unl.edu.ar, eferrante@sinc.unl.edu.ar).

Tom Tirer is with the Faculty of Engineering, Bar-Ilan University, Ramat Gan 5290002, Israel (e-mail: tirer.tom@gmail.com).

Lucas Mansilla is with Universidad Nacional del Litoral, Santa Fe, Argentina (e-mail: lmansilla@sinc.unl.edu.ar).

Gabriel Jimenez and Guanghui Fu are with Sorbonne Université, Institut du Cerveau - Paris Brain Institute - ICM, CNRS, Inria, Inserm, AP-HP, Hôpital de la Pitié Salpêtrière, Paris, France - RRID:SCR_026393 (emails: gabriel.jimenez@icm-institute.org, guanghui.fu@icm-institute.org).

truth (GT) labels. Commonly used metrics include the Dice-Sørensen coefficient (DSC) and other overlap-based measures [1], as well as distance-based metrics, such as the Hausdorff distance or the average symmetric surface distance (ASSD) [2], [3].

Once a segmentation method is deployed in practice, continuously assessing its real performance on new unseen data samples becomes a challenging task, mainly due to the limited availability of reference annotations in clinical settings. However, evaluation remains a critical task, especially for identifying instances where an image segmentation method may fail in automatic pipelines due to unexpected changes, e.g. in patient demographics [4] or acquisition protocols. This motivates the development of methods that can automatically estimate segmentation quality when no ground truth is available.

Reverse Classification Accuracy (RCA) [5] is a framework originally designed to predict the performance of an image segmentation method in scenarios where GT masks are unavailable. It works by using the predicted segmentation of a new image as a pseudo-ground truth to train a reverse classifier (a segmentation network in our case)¹. This model is then applied to a set of reference images with known GT, and its performance is evaluated using standard metrics like the DSC. The distribution of scores over the reference set serves as a proxy for the quality of the original segmentation. Even though RCA has been widely adopted in the medical imaging community, it still suffers from two main limitations: it is very inefficient in computational terms and it lacks a mechanism to understand how reliable the estimated segmentation performance is. In this work, we focus on addressing both limitations by proposing a flexible approach that combines recent advances in In-Context Learning (ICL) for segmentation [6], with split conformal prediction [7], [8] to build confidence intervals for the estimated metrics.

We first introduce In-Context RCA, which leverages incontext learning segmentation models [9], [10] that can perform new tasks by conditioning on a small set of labeled examples without requiring any additional training. In the context of image segmentation, this means we can segment a new image by simply providing a few example image-mask

¹Note that we use the term *reverse classifier* as introduced in the original publication [5], although it would be more accurately described as a *reverse segmenter*. We will use both terms interchangeably.

pairs, avoiding the need to train a new segmentation model. By leveraging in-context segmentation models as reverse classifiers, our framework makes the process more efficient and practical for clinical use.

More importantly, we address a key limitation that is shared across most existing segmentation quality control frameworks: the lack of statistical guarantees for the estimated quality scores. Traditionally RCA yields a single point estimate of segmentation quality, such as the mean or maximum over the set of reference scores. While useful, this estimate does not express the uncertainty inherent in the prediction. In this work, we propose to generate confidence intervals by incorporating tools from split conformal prediction [7], [8], [11], which provide statistical guarantees that the intervals contain the true segmentation score with a user-specified probability. This results in a more informative and reliable assessment of segmentation quality, going beyond point estimates to quantify uncertainty at the individual image level.

II. RELATED WORK

A. InContext Learning and Reverse Classification Accuracy

Despite its relevance, few approaches have addressed automatic quality control of segmentations thus far. Many previous works have relied on extracting features from segmentations and fitting a model to these features. Such approaches have been applied to prostate segmentation [12], cardiac segmentation [13], and a more generic framework has been used to assess the quality for automated segmentations for lung and liver in [14]. However, these methods are constrained by the feature extraction, which can limit their adaptability and generalizability to diverse clinical data. Additionally, a CNN-based approach was developed for automated quality control of left ventricle segmentation in cardiac MRI [15]. In spite of demonstrating the potential of deep learning for automatic quality assessment, this method requires generating a synthetic dataset and further training multiple CNN models.

Other previous studies rely on a reverse-testing strategy, where a new classifier is trained on predictions on the test data and evaluated again on the training data [16]-[18]. The limitation of these approaches is that they only provide an estimate of the average performance rather than case-specific estimations. Building on this idea, Reverse Classification Accuracy (RCA) has been shown to provide accurate predictions of segmentation quality on a per-image basis [5], [19]. In [5], Atlas-based segmentation has shown to be the most effective reverse classifier for medical image segmentation. However, the computational time required to complete atlas based segmentation on a single instance is a limitation, making it impractical for real-time quality control. In [20] the authors propose using a neural network to directly estimate prediction quality, aiming to mitigate the time constraint. However, this approach necessitates training a separate CNN for each task, which significantly limits its practicality and scalability. More importantly, both methods [5], [19] have only been used for anatomical segmentation and not for lesions, which are usually more challenging due to the lack of regularity.

Recently, Few-shot Semantic Segmentation (FSS) methods —which extend in-context learning to address segmentation

tasks— have shown great potential in the medical domain, particularly with limited annotations [21]. While traditional approaches are often based on prototypical networks [22], [23], more advanced models such as UniverSeg [9] and foundational models like SAM 2 [10], [24], [25] delivered more promising results on a wide range of medical tasks. This enhanced generalizability is largely due to their training on vast amounts of diverse data. Here we will use FSS to improve RCA performance and efficiency.

B. Performance Interval Estimation

While most existing methods for segmentation quality estimation focus on predicting point estimates, few works aim to quantify the uncertainty of such estimations. Recently, the idea of estimating performance ranges has emerged as a promising direction. One notable approach is the method proposed in [26], which applies split conformal prediction to produce intervals for segmentation quality scores with formal coverage guarantees. To do so, however, they must either train specialised probabilistic segmentation models that can sample multiple plausible outputs for the same input—such as Probabilistic U-Net [27] or PHiSeg [28]—or rely on alternative uncertainty estimation techniques like test-time augmentation [29], Monte-Carlo dropout [30], or ensembling [31]; all of which add further implementation overhead and yielded lower performance in the reported experiments. In addition, the method constructs its intervals from nonconformity scores based on the softmax scores [32], [33], which are known to suffer from calibration issues [34], [35]. In this work, we introduce Conformal RCA, which is model-agnostic and can be used to estimate quality intervals for segmentation masks regardless of the underlying architecture or training procedure used to produce them. Unlike [26], we base our conformal prediction framework on Conformalized Quantile Regression (CQR), leveraging its ability to produce tighter prediction intervals than alternative conformal approaches commonly used for regression [11], and introducing novel modifications tailored to the RCA procedure.

Our Contributions:

- We propose In-Context RCA, extending the traditional RCA framework by leveraging in-context segmentation models as reverse classifiers. These models adapt their predictions using a few labeled examples at inference time, without requiring additional training.
- We introduce Retrieval-Augmented RCA, a more efficient variant of RCA that uses embedding-based retrieval to select the most relevant reference images to be used as few-shot examples, enhancing efficiency and accuracy.
- We propose to incorporate conformal prediction into RCA for the first time, enabling the estimation of prediction intervals with statistical guarantees, and providing imagelevel uncertainty quantification. We base our approach on CQR, but unlike prior work that trains a quantile regression model, we estimate the quantiles directly from the RCA reference set, avoiding additional training.

 We conduct extensive experiments on 10 diverse medical imaging datasets, demonstrating strong performance across different modalities and anatomy. We significantly broaden the scope of RCA while reducing inference time.

III. IN-CONTEXT RCA

Suppose we deployed to production an X-ray lung segmentation model, and we want to monitor the quality of the segmentation S_I produced for a new image I. Let us also assume access to a reference database $D = \{(J_i, S_{J_i}^{GT})\}_{i=1}^m$ of annotated images (in our case, X-ray images with expert annotations). The core idea behind RCA is to assess the quality of a segmentation S_I corresponding to a new image I by training a reverse segmenter f_{I,S_I} (or reverse classifier) using only S_I as pseudo-ground truth for training. The reverse segmenter is then applied to each image in D, generating segmentations $f_{I,S_I}(J_i) = S_{J_i}$. The quality of these segmentations is then assessed by computing a chosen quality metric ρ (e.g DSC) for each S_{J_i} and its corresponding ground truth $S_{J_i}^{GT}$. This process yields a set of scores:

$$\mathcal{Y} = \left\{ y^{(k)}(S_I) = \rho(S_{J_k}, S_{J_k}^{GT}) \right\}_{k=1}^m. \tag{1}$$

Traditionally, RCA collapses this set into a point estimate of segmentation quality by taking the best metric value (or the mean) over \mathcal{Y} :

$$\hat{\rho}(S_I) = \max_k \rho(S_{J_k}, S_{J_k}^{GT}), \tag{2}$$

assuming that higher values of ρ correspond to better quality estimations. The underlying hypothesis is that if S_I is of high quality, the RCA segmenter should perform well on at least some of the reference images, resulting in high values of ρ . Conversely, if S_I is of poor quality, the segmenter is expected to perform poorly on the reference database.

In this work, we propose to adopt in-context segmentation models as reverse segmenters, resulting in In-Context RCA (see Fig. 1). Unlike previous approaches, that rely on training CNNs [20] or computationally expensive atlas-based registration methods as reverse classifiers [5], [19], in-context learning models are computationally efficient and can adapt their predictions based on a small support set. We also introduce a dynamic selection of the reference dataset on a per-case basis based on retrieval similarity, enabling the use of smaller, more relevant reference datasets. Here we employ two different reverse in-context segmenters to demonstrate the approach's versatility.

UniverSeg-based reverse segmenter. The UniverSeg architecture [9] was designed to tackle unseen medical segmentation tasks without requiring additional training. Given a query image Q and a small support set $\mathcal S$ of image-label pairs that define a new segmentation task, UniverSeg is able to segment the query image Q following the provided examples, without updating the neural weights. It follows a UNet-like encoder-decoder architecture composed of CrossBlock modules. These modules, which are convolutional layers, enable the transfer of relevant information between the support set and the query image, allowing the model to perform accurate segmentation

without task-specific retraining. It was trained on a collection of 53 open-access medical segmentation datasets called MegaMedical, covering a wide range of image modalities and structures.

Here we adopt UniverSeg as the reverse classifier of the In-Context RCA framework. To this end, we use the target image I and the predicted segmentation under assessment S_I as the UniverSeg support set, i.e. we simply define $S = \{(I, S_I)\}$. We then segment all the reference images J_i in our RCA reference database by considering them as query images, one at a time, and finally compare each resulting segmentation S_{J_k} with the corresponding reference segmentation $S_{J_k}^{GT}$ to estimate $\hat{\rho}(S_I)$ as defined in Eq. (2).

SAM 2-based reverse segmenter. Segment Anything Model (SAM) [36] is a foundation model for image and video segmentation guided by prompts. Its architecture consists of image and prompt encoders that extract features, and a mask decoder that fuses this information to generate segmentations. SAM 2 [24] extends its predecessor by incorporating memory components (an encoder, bank, and attention mechanism) enabling adaptation to new tasks and outperforming existing video object segmentation models, especially for temporal tracking. For medical FSS [25], SAM 2 treats the support set as initial frames of a sequence, with their segmentation masks serving as prompts. Despite having no temporal connection between images, this approach effectively transfers segmentation masks from annotated to unannotated examples (see [25] for more details). In our framework, we use SAM 2 as a reverse classifier, following the few-shot setting with sequences that comprise only two frames: 1) the target image and its pseudoground truth, and 2) a query image drawn from the reference dataset.

A. Retrieval Augmented (RA)-RCA

In order to further improve the efficiency of RCA, we propose to reduce the size of the RCA reference database by dynamically retrieving the most relevant reference images on a per-case basis. This allows the model to focus on smaller, more relevant subsets of data, optimizing computational efficiency while maintaining and even improving the quality of predictions. To implement this, we embed all the images from the reference database using DINOv2 embeddings [37] and then create a vector database using FAISS [38], which enables efficient similarity search. For each incoming target image whose segmentation quality we want to assess, we compute its embedding and retrieve the k most similar images from the reference index based on cosine similarity. While DINOv2 was not explicitly trained for the medical domain, it has shown strong generalization, making it effective for general tasks, including those in medical imaging. In fact, a similar retrievalaugmented approach for few-shot medical image segmentation has been explored in [39], demonstrating its effectiveness in similar scenarios. In the case of X-ray images, we leverage RAD-DINO [40], a domain-specific version of DINOv2 finetuned for radiology, as we expect it to further improve performance.

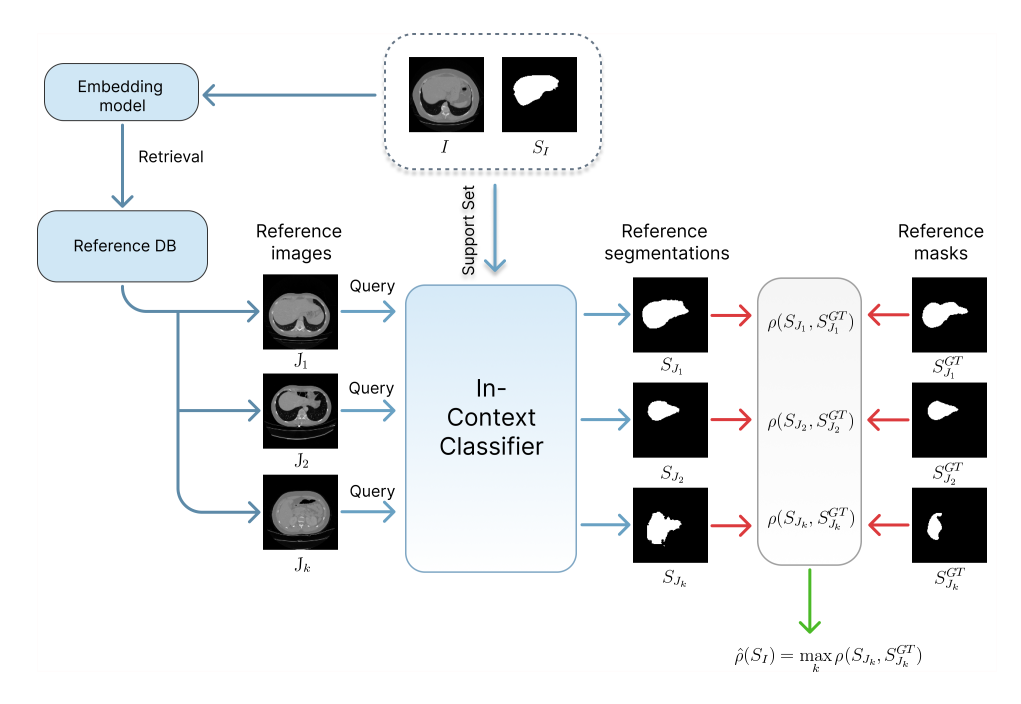


Fig. 1. General outline of the In-Context RCA framework. The quality of a predicted segmentation S_I on an image I is estimated by leveraging (I, S_I) as the support set of an In-Context Classifier or segmenter. This classifier is then applied to segment a reference dataset, selected through retrieval augmentation. Finally, the best segmentation result based on an evaluation metric ρ , is used to predict the quality of S_I following Eq. (2).

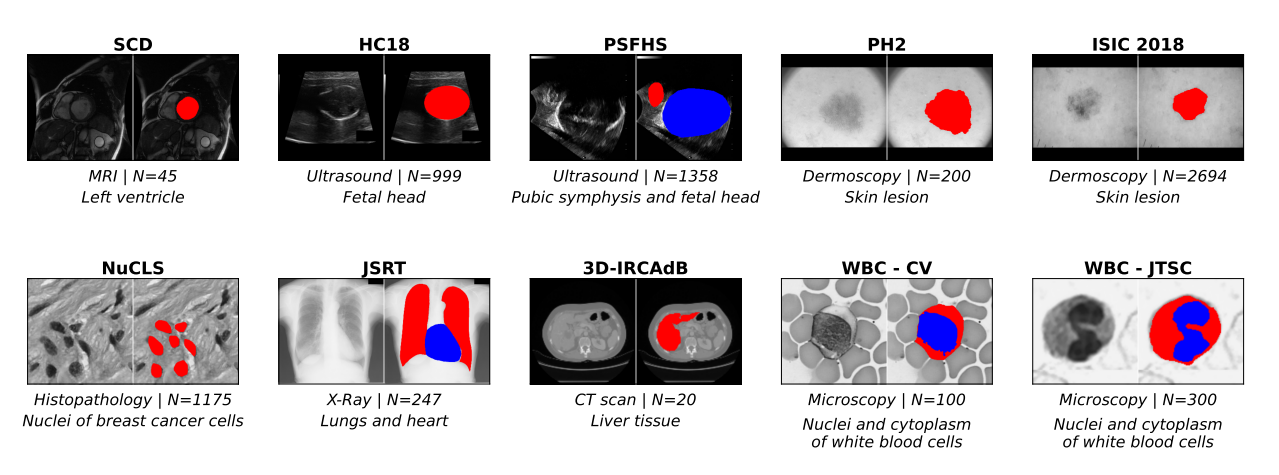


Fig. 2. Datasets overview including modality, number of images and structure.

IV. CONFORMAL RCA

A. Preliminaries: Split Conformal Prediction

Conformal Prediction (CP) is a model-agnostic, distribution-free framework for uncertainty quantification that provides statistically valid prediction sets or intervals, for classification and regression tasks respectively, under minimal assumptions [7], [8]. Given a desired coverage level $1-\alpha$ with $\alpha \in (0,1)$ and a "nonconformity score" function, CP constructs a prediction region $C_{\alpha}(X)$ for a given sample X such that $Y \in C_{\alpha}(X)$ with probability $1-\alpha$, where Y is the true label. Here, the desired coverage level $1-\alpha$ specifies the proportion of times the true outcome is expected to fall within the prediction set, while the nonconformity score quantifies how unusual or "nonconforming" a candidate prediction is with respect to the observed data.

We focus on *split conformal prediction*, a practical variant that conformalizes a fixed model using a held-out calibration set. This contrasts with *full conformal prediction*, which typically requires retraining the model for each new test point. The only required assumption is that the calibration samples and the test samples are exchangeable (e.g., the samples are i.i.d.). Let us now state the general procedure for split conformal prediction, as presented in [8]. Given a calibration set $\{(x_i, y_i)\}_{i=1}^n$ and a new test input x_{n+1} :

- 1. Define a nonconformity score function $s(x,y) \in \mathbb{R}$ that quantifies the disagreement between the model's prediction for input x and a ground-truth label y (e.g. the absolute difference between the predicted and expected DSC score). Higher scores indicate poorer fit or higher error.
- 2. Compute \hat{q} as the $\lceil (1-\alpha)(1+1/n) \rceil$ -th empirical quantile

of the calibration scores $\{s(x_1,y_1),\ldots,s(x_n,y_n)\}$. For example, for a desired coverage of 90% ($\alpha=10\%$), \hat{q} will be the nonconformity score under which 90% of the nonconformity scores computed in the calibration set fall.

3. Construct the prediction set for x_{n+1} as:

$$C_{\alpha}(x_{n+1}) = \{y : s(x_{n+1}, y) \le \hat{q}\}.$$

This set (or interval in case of regression problems) will contain all candidate outputs for x_{n+1} that have a nonconformity score less than or equal to the threshold.

This procedure gives the following coverage guarantee:

Theorem 1. Suppose that $\{(X_i, Y_i)\}_{i=1}^n$ and (X_{n+1}, Y_{n+1}) are i.i.d. Let \hat{q} and $C_{\alpha}(X_{n+1})$ be as defined above. Then the following holds:

$$\mathbb{P}(Y_{n+1} \in C_{\alpha}(X_{n+1})) \ge 1 - \alpha. \tag{3}$$

The proof of this result traces back to [7]. Although the coverage guarantee holds regardless of the score function, the usefulness of the prediction sets is determined by how well it captures the model's uncertainty. In practice, conformal prediction methods are primarily evaluated in terms of *validity* (i.e., achieving the desired coverage level) and *efficiency* (i.e., producing prediction sets or intervals that are as tight as possible).

In regression problems, a widely adopted nonconformity score is the residual $s(x,y)=|y-\hat{f}(x)|$, where $\hat{f}(x)$ denotes the model's prediction for input x [7]. The resulting conformal prediction interval takes the form $C_{\alpha}(x_{n+1})=\hat{f}(x_{n+1})\pm\hat{q}$. Note that this leads to prediction intervals of equal width for all test inputs, regardless of their location in the input space. To better account for heteroscedasticity, i.e. when the noise variance varies across the input domain, a locally weighted nonconformity score has been proposed: $s(x,y)=\frac{|y-\hat{f}(x)|}{\hat{\sigma}(x)}$, where $\hat{\sigma}(x)$ is the estimated standard error of the residual [41].

An alternative and popular approach that naturally accounts for heteroscedasticity is Conformalized Quantile Regression (CQR) [11]. CQR, builds on quantile regression models, which are trained to predict the conditional lower and upper quantiles $\hat{t}_{\alpha/2}(x)$ and $\hat{t}_{1-\alpha/2}(x)$ of the response Y given an input X=x. The nonconformity score is defined as the distance from y to the nearest quantile:

$$s(x,y) = \max \{\hat{t}_{\alpha/2}(x) - y, \ y - \hat{t}_{1-\alpha/2}(x)\}$$

and the prediction interval for a new input x_{n+1} is constructed as:

$$C_{\alpha}(x_{n+1}) = \left[\hat{t}_{\alpha/2}(x_{n+1}) - \hat{q}, \ \hat{t}_{1-\alpha/2}(x_{n+1}) + \hat{q}\right].$$

We build on the CQR framework as the basis for our proposed method. This approach maintains the coverage guarantee of CP while often producing tighter, more locally adaptive intervals compared to residual-based methods, particularly in heteroscedastic settings [11].

B. Proposed Method

Traditional RCA yields a point estimate of segmentation quality for an individual image, as defined in Eq. (2). However, it does not quantify the uncertainty associated with this prediction. To address this limitation, we extend RCA following a split conformal prediction approach, producing prediction intervals with statistical guarantees.

Let $\mathcal{C}=\{(I_j^C,S_{I_j^C},S_{I_j^C}^{GT})\}_{j=1}^n$ be a calibration set of images with both predicted $(S_{I_j^C})$ and ground-truth $(S_{I_j^C}^{GT})$ segmentations. For each calibration sample $(I_j^C,S_{I_j^C})$, we apply the RCA procedure: we train a reverse segmenter $f_{I_j^C,S_{I_j^C}}$ using $S_{I_j^C}$ as pseudo-ground truth, evaluate it on the reference database D, and obtain the corresponding RCA scores \mathcal{Y}_j^C following Eq. (1). We also compute the true quality score $y(S_{I_j^C}) = \rho(S_{I_j^C}, S_{I_j^C}^{GT})$ of each sample in the calibration set.

To construct the prediction intervals, we follow an approach inspired by CQR but differing in a key aspect: instead of training a quantile regression model, we compute empirical quantiles directly from the RCA score distribution \mathcal{Y} . This allows us to naturally capture the uncertainty inherent in the RCA procedure while maintaining computational efficiency.

From each RCA score distribution \mathcal{Y}_j^C , we compute empirical quantiles at asymmetric levels that are chosen to reflect RCA's characteristic behavior. Specifically, the lower quantile $q_\ell(S_{I_j^C}) = \operatorname{Quantile}(\mathcal{Y}_j^C, p_\ell)$ is selected near the center of the distribution, while the upper quantile $q_h(S_{I_j^C}) = \operatorname{Quantile}(\mathcal{Y}_j^C, p_h)$ is chosen closer to the maximum. This asymmetry captures the observation that RCA tends to underestimate segmentation quality, making higher scores more informative [5].

We then define nonconformity scores that measure how far the true quality deviates from the RCA-based interval bounds:

$$s_j = \max\{q_{\ell}(S_{I_i^C}) - y(S_{I_i^C}); \ y(S_{I_i^C}) - q_h(S_{I_i^C})\}. \tag{4}$$

Based on the calibration nonconformity scores, $\{s_j\}_{j=1}^n$, the "CP threshold", \hat{q} , is computed as the $\lceil (1-\alpha)(1+1/n) \rceil$ -th smallest value among $\{s_j\}_{j=1}^n$ (see Step 2 in Section IV-A). For a new test pair (I,S_I) , we compute its RCA scores $\mathcal Y$ and compute the corresponding empirical quantiles $q_\ell(S_I)$ and $q_h(S_I)$. The conformalized prediction interval is then constructed as:

$$C(S_I) = [q_{\ell}(S_I) - \hat{q}, q_h(S_I) + \hat{q}]. \tag{5}$$

Assuming exchangeability between the test sample and calibration set, the constructed interval provides the marginal coverage guarantee stated in Theorem 3, as shown in [11]. In our experiments, ρ corresponds to the Dice Similarity Coefficient (DSC), which takes values in the [0,1] range. Accordingly, we clip the predicted interval $C(S_I)$ to this range to ensure plausible quality estimates. Note that the procedure can be applied with any reverse segmenter and can thus be readily combined with the proposed in-context approach.

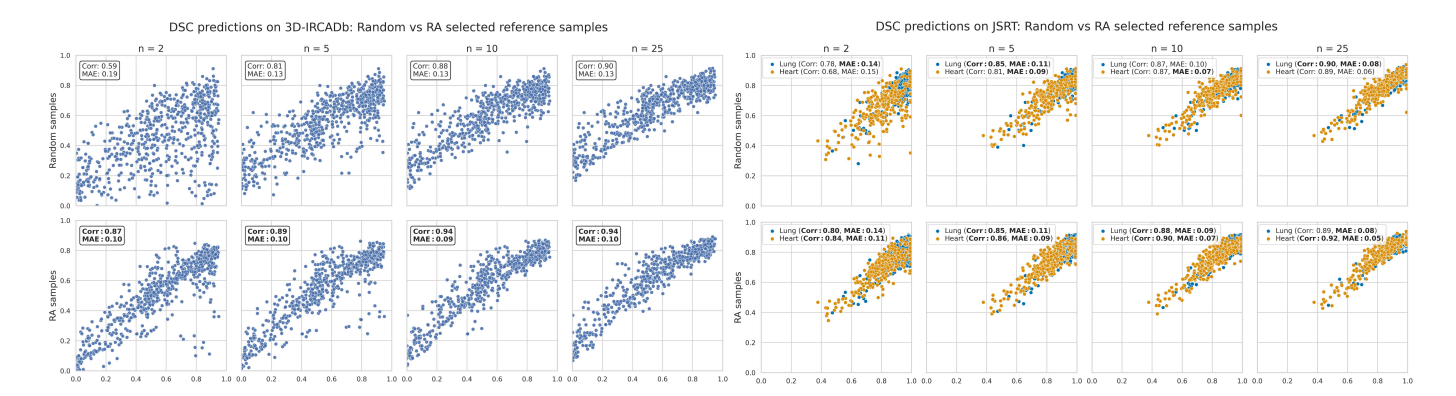


Fig. 3. Scatter plots comparing predicted vs real DSC on 3D-IRCAdB (**Left**) and JSRT (**Right**) for different reference datasets of size k using UniverSeg as the reverse classifier. **Top**: results using randomly selected reference samples. **Bottom**: results following retrieval-augmentation, where the k most similar images are selected based on cosine similarity in the DINOv2 embedding space. In both cases retrieval-augmentation achieves better performance with fewer samples, as shown by higher correlation and lower MAE (bold indicates the best value).

V. EXPERIMENTS AND RESULTS

A. Datasets & Computing Resources

We evaluate the proposed Conformal and In-Context RCA variants across diverse datasets listed in Fig. 2 including SCD [42], HC18 [43], PSFHS [44], PH2 [45], ISIC 2018 [46], NuCLS [47], JSRT [48], 3D-IRCAdB [49], WBC-CV and WBC-JTSC [50]. Unlike previous studies that explored RCA focusing on cardiac MRI [19], [20] or multi-organ segmentation on whole-body MRI [5] only, we broaden our analysis to a wider range of medical imaging challenges. To maintain consistency, we convert all images to grayscale and resize them to 256x256 pixels. For 3D images, we extract slices, keeping those where the region of interest (ROI) is present.

All the experiments that will be described here were conducted on an AMD Ryzen 7 4800H CPU (8 cores) and an NVIDIA GTX 1660 Ti GPU (6GB of VRAM).

B. Evaluation of In-Context RCA

Simulating masks of diverse quality. To evaluate In-Context RCA, we generate segmentation masks of varying quality by training a small U-Net [51] for 10 epochs and saving the lower and higher-quality segmentations. Our goal is to achieve a uniform distribution of mask qualities with varying DSC for a comprehensive evaluation.

Impact of dataset size and RA on performance. We evaluate the impact of the reference dataset size and the use of RA (retrieval augmentation) by applying In-Context RCA with UniverSeg as our reverse classifier, considering different support set sizes. We aim to determine if RA maintains or even improves prediction quality while using a smaller reference dataset, thus reducing inference time in practice. We considered reference dataset sizes of 2, 5, 10 and 25 examples. Larger sets noticeably increase inference time per image without any meaningful improvement in prediction accuracy. Since UniverSeg supports only binary segmentation, for multiclass we process them separately (including background), and then select the most likely class per pixel using softmax, as described in [9].

Fig. 3 shows the results on 3D-IRCAdB and JSRT datasets, comparing the performance of In-Context RCA for different reference datasets of size k. The figure contrasts two selection methods: random selection (first row) and RA (second row), where the k most similar images are chosen based on cosine similarity in the DINOv2 embedding space. The horizontal axis represents the predicted DSC, while the vertical axis shows the real value. As the number of reference samples increases, both methods show improved performance, yielding higher correlation and lower mean absolute error (MAE). However, RA achieves better results with fewer reference samples, what is particularly beneficial during deployment, as it reduces inference time. Other similarity metrics, such as Euclidean distance and inner-product were also considered, but cosine similarity showed the best results.

Comprehensive evaluation across datasets. In order to assess the effectiveness and limitations of In-Context RCA, we conducted an extensive evaluation using UniverSeg and SAM 2 as reverse classifiers, considering DSC as evaluation metric. We compared the performance of In-Context RCA with a singleatlas approach, known to offer the strongest results in the classical RCA framework [5], [19]. For the atlas, we included both traditional and RA versions, whereas for UniverSeg and SAM 2, we focused exclusively on the RA version as it showed better pefromance in our previous experiment (see Fig. 3). We used the segmentation masks generated by a UNet trained for different epochs as previously discussed, to ensure evaluation across varying segmentation qualities. We observe that following RA reference sample selection yields good results without requiring a large reference database. In all cases, we fixed the size of the reference dataset to 8, based on previous observations.

Fig. 4 provides a comprehensive overview of the results when predicting the DSC across all datasets for all four variants: the traditional RCA framework using single-atlas, its RA version, and the In-Context RCA methods using UniverSeg and SAM 2 as reverse classifiers. We observe that In-Context RCA demonstrates similar and, in some cases, better results compared to the Atlas method, while being

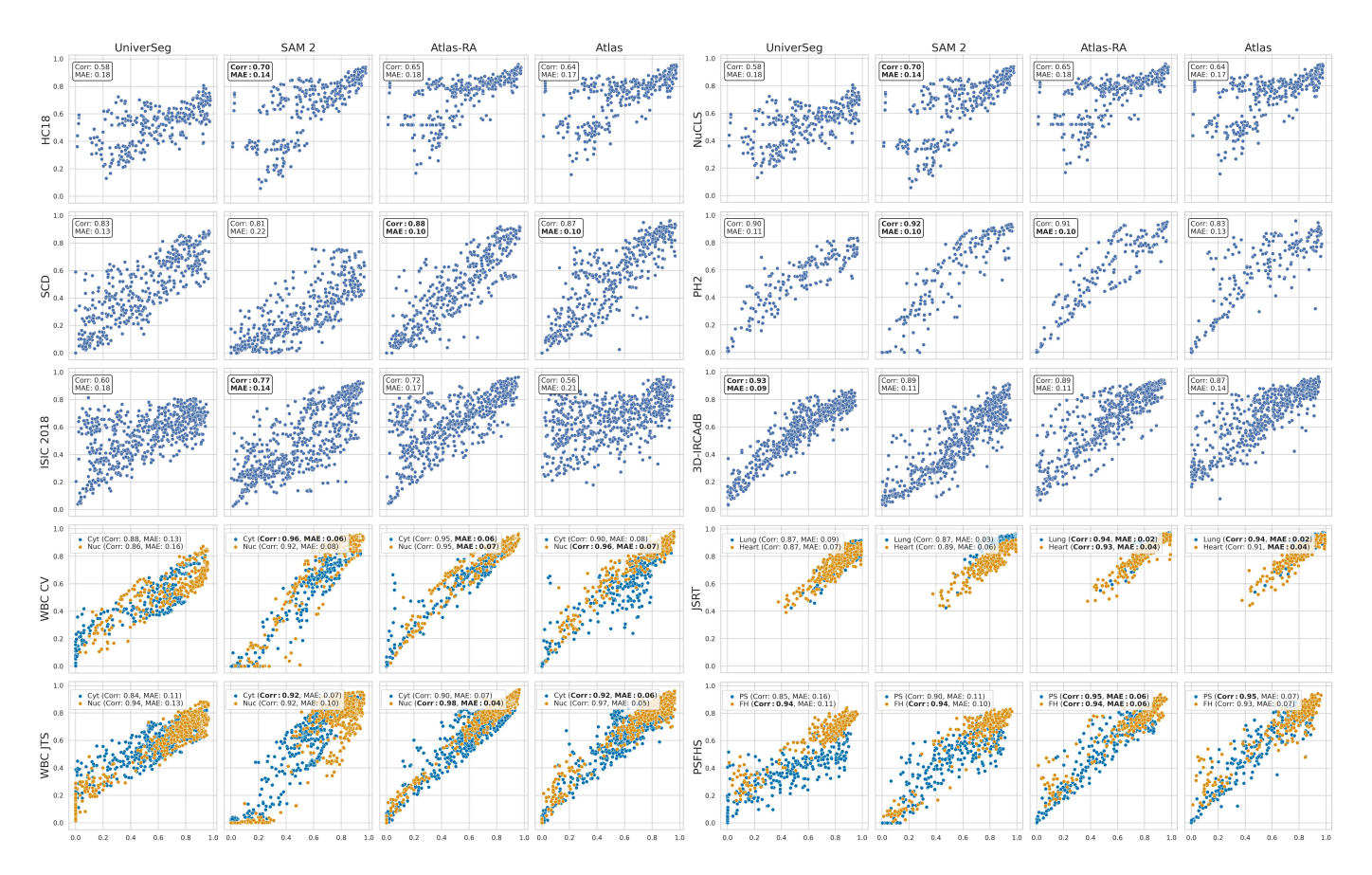


Fig. 4. Scatter plots comparing the predicted DSC across all datasets for In-Context RCA using UniverSeg and SAM 2 as reverse classifiers, followed by the retrieval-augmented and traditional Atlas RCA versions. All evaluations were conducted with a reference dataset of size 8. Bold indicates the winning method per dataset.

significantly more computationally efficient. Particularly in highly irregular segmentation problems like the NuCLS histopathology dataset, our SAM2 variant achieves good correlation of about 0.70 while Atlas methods completely fail.

Performance gains for In-Context RCA. Importantly, while the classic RCA-atlas method takes on average one minute to process each image, SAM 2 and UniverSeg achieve the same task in just 0.70 seconds and 0.37 seconds respectively, approximately 85 and 162 times faster. This efficiency, combined with its strong performance, makes In-Context RCA an ideal choice for integration into clinical pipelines.

C. Evaluation of Conformal RCA

To evaluate our conformal RCA approach, we split each dataset into training (80%), calibration (10%) and test (10%) subsets. The calibration set is used to compute the CP threshold \hat{q} that adapts the prediction intervals, while performance is reported on the held-out test set.

In order to enable direct comparison with [26], we adopt PHiSeg [28]—the top performer in that work—as our backbone segmentation model. Importantly, Conformal-RCA remains model-agnostic, making it applicable to any underlying segmentation network regardless of output format. Segmentation masks of varying quality for both calibration and test

sets were generated by training PHiSeg and saving intermediate checkpoints, following the same procedure as before. For PHiSeg, we follow the conformal calibration procedure described in [26]: for each input image, N=50 stochastic segmentations are generated, and the DSC is estimated from the softmax outputs [32], yielding a distribution of predicted DSCs per sample. Nonconformity scores are defined as the absolute residuals between the mean predicted and ground truth DSC, scaled by the empirical standard deviation of the distribution. We additionally explore PHiSeg (CQR), a newly proposed variant where nonconformity scores are computed following the empirical CQR method. In this case, empirical quantiles are computed at levels 0.2 and 0.8.

Fig. 5 reports the distribution of prediction interval sizes and empirical coverage levels across all datasets for the evaluated methods. We include different versions of our approach, which differ only in the choice of reverse segmenter: the classical atlas-based method, and our two proposed in-context learning-based alternatives—UniverSeg and SAM 2. For all variants, we used a reference database of size 32, selected following the RA approach previously described. Empirical quantiles were computed at levels $p_{\ell}=0.4$ and $p_h=0.95$ and prediction intervals were constructed with a user-specified coverage of 90% ($\alpha=0.1$) as described in Section IV-B.

Panel (a) of Fig. 5 shows the distribution of prediction interval widths across all datasets. Among our Conformal-RCA

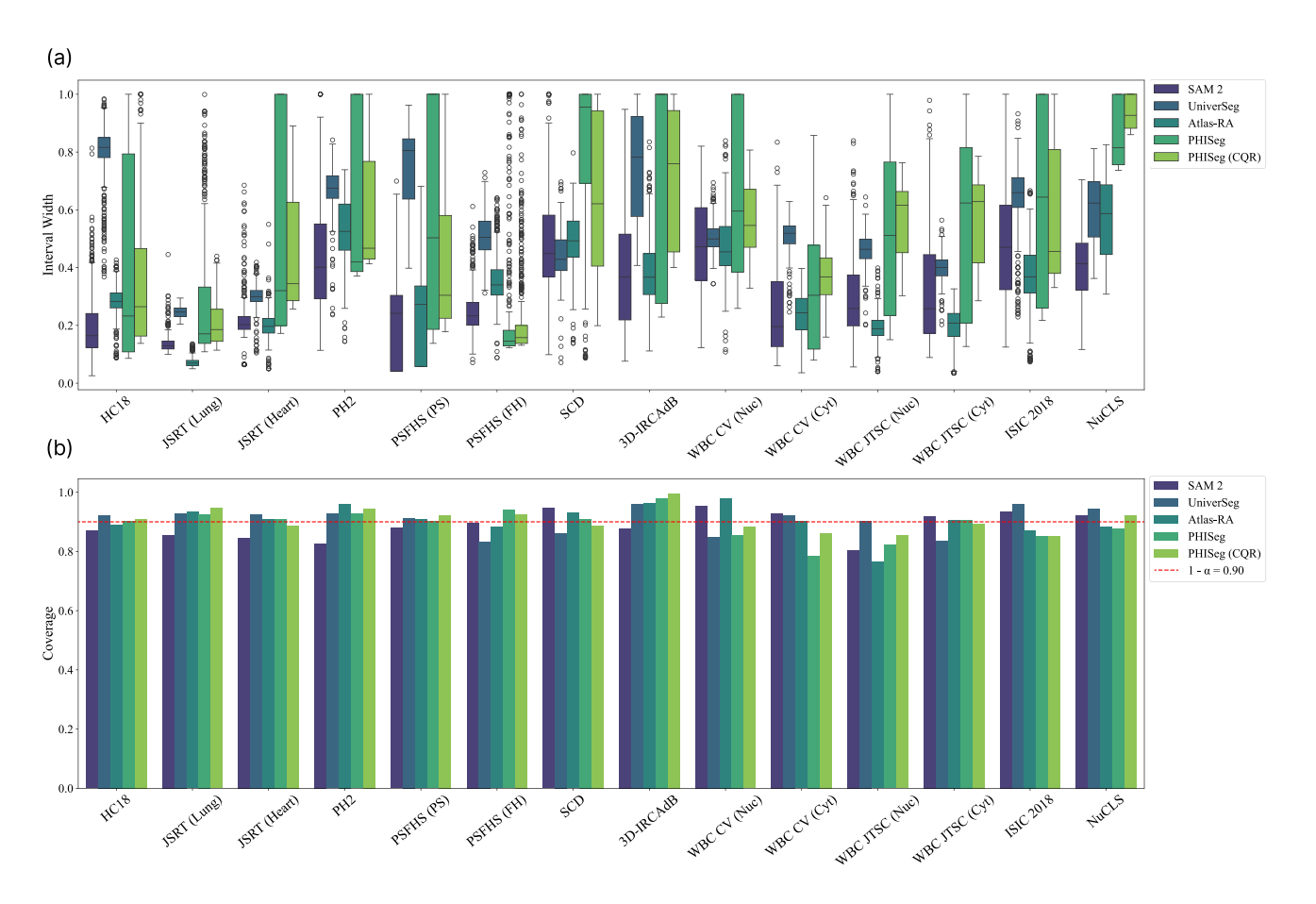


Fig. 5. (a) Distribution of prediction interval sizes (the lower the better) and (b) empirical coverage rates (the larger the better) for conformal prediction methods across all evaluated datasets. Results compare our Conformal-RCA variants using different reverse segmenters (Atlas-based, UniverSeg, SAM 2) against the baseline method PHiSeg from [26], as well as our proposed variant PHiSeg (CQR), which follows the empirical CQR approach. Target coverage level is set to 90% ($\alpha = 0.1$).

variants, SAM 2 and Atlas achieve consistently tight intervals, whereas UniverSeg yields somewhat wider intervals. Notably, SAM 2 offers a substantial computational speed-up over the atlas-based approach while maintaining similar interval quality. Compared to the PHiSeg baseline, UniverSeg occasionally produces wider intervals; however, both SAM 2 and Atlas consistently attain lower median widths and reduced spread, indicating more robust uncertainty quantification. Importantly, compared to the conformal procedure used in prior work [26], the CQR variant of PHiSeg produces tighter intervals, further highlighting the benefits of following our proposed empirical CQR method within the CP framework.

As shown in panel (b) of Fig. 5, neither our Conformal-RCA nor the PHiSeg variants consistently reach the target marginal coverage of 90%. This under-coverage phenomenon was also observed in [26] and is likely due to violations of the exchangeability assumption between the test and calibration splits. To further support this hypothesis, we ran controlled experiments in which both calibration and test sets are drawn from the same known distribution. In these controlled settings where the exchangeability assumption holds, the desired nominal coverage level of 90% is achieved (see Appendix).

VI. CONCLUSION

In this work, we addressed the critical challenge of evaluating medical image segmentation quality in the absence of ground truth by presenting two complementary frameworks. First, In-Context RCA leverages the power of in-context segmentation models as reverse classifiers and integrates retrieval augmentation to select relevant reference samples. This combination enables efficient quality estimation using smaller reference databases while either matching or improving prediction accuracy of traditional RCA.

Second, Conformal RCA extends the traditional RCA procedure using split conformal prediction to produce prediction intervals with statistical guarantees, providing a more comprehensive assessment of segmentation quality that moves beyond point estimates. Unlike previous interval-estimation approaches that rely on specialized probabilistic architectures and require calibrated softmax outputs, Conformal RCA is fully model-agnostic and easily integrates with any segmentation network.

Experimental results conducted across diverse medical imaging modalities, show that In-Context RCA achieves comparable or superior performance to traditional atlas-based approaches while being up to two orders of magnitude faster. It also overcomes the limitations imposed by atlas-based

methods allowing to tackle scenarios beyond anatomical segmentation, such as cell images. Conformal RCA demonstrates the ability to produce meaningful prediction intervals that outperform existing conformal prediction approaches for segmentation quality control.

A remaining limitation is the reliance of exchangeability between calibration and test sets. When this assumption is violated (e.g., due to domain shifts in scanner settings or patient populations), coverage can degrade. Developing methods that are robust to distribution shifts is an important direction for future work.

Overall, our results position both In-Context RCA and Conformal RCA as promising and practical solutions for automated quality control in clinical workflows, where rapid and reliable segmentation assessment is essential.

REFERENCES

- W. R. Crum, O. Camara, and D. L. Hill, "Generalized overlap measures for evaluation and validation in medical image analysis," *IEEE transactions on medical imaging*, vol. 25, no. 11, pp. 1451–1461, 2006.
- [2] D. Müller, I. Soto-Rey, and F. Kramer, "Towards a guideline for evaluation metrics in medical image segmentation," *BMC Research Notes*, vol. 15, no. 1, p. 210, 2022.
- [3] A. A. Taha and A. Hanbury, "Metrics for evaluating 3d medical image segmentation: analysis, selection, and tool," *BMC medical imaging*, vol. 15, pp. 1–28, 2015.
- [4] N. Gaggion, R. Echeveste, L. Mansilla, D. H. Milone, and E. Ferrante, "Unsupervised bias discovery in medical image segmentation," in Workshop on Clinical Image-Based Procedures. Springer, 2023, pp. 266– 275
- [5] V. V. Valindria, I. Lavdas, W. Bai, K. Kamnitsas, E. O. Aboagye, A. G. Rockall, D. Rueckert, and B. Glocker, "Reverse classification accuracy: Predicting segmentation performance in the absence of ground truth," *IEEE transactions on medical imaging*, vol. 36, no. 8, p. 1597—1606, 2017
- [6] X. Wang, X. Zhang, Y. Cao, W. Wang, C. Shen, and T. Huang, "Seggpt: Towards segmenting everything in context," in *Proceedings of the IEEE/CVF International Conference on Computer Vision (ICCV)*, 2023, pp. 1130–1140.
- [7] V. Vovk, A. Gammerman, and G. Shafer, Algorithmic Learning in a Random World. Springer-Verlag, 2005.
- [8] A. N. Angelopoulos and S. Bates, "A gentle introduction to conformal prediction and distribution-free uncertainty quantification," 2022.
- [9] V. I. Butoi, J. J. G. Ortiz, T. Ma, M. R. Sabuncu, J. V. Guttag, and A. V. Dalca, "Universeg: Universal medical image segmentation." in *ICCV*. IEEE, 2023, pp. 21 381–21 394.
- [10] J. Zhu, Y. Qi, and J. Wu, "Medical sam 2: Segment medical images as video via segment anything model 2," CoRR, vol. abs/2408.00874, 2024
- [11] Y. Romano, E. Patterson, and E. Candes, "Conformalized quantile regression," in *Advances in Neural Information Processing Systems*, vol. 32. Curran Associates, Inc., 2019.
- [12] M. R. Sunoqrot et al., "A quality control system for automated prostate segmentation on t2-weighted mri," *Diagnostics*, vol. 10, no. 9, p. 714, 2020
- [13] Y. Xu et al., "Automated quality control for segmentation of myocardial perfusion spect," *Journal of Nuclear Medicine*, vol. 50, no. 9, pp. 1418– 1426, 2009.
- [14] T. Kohlberger, V. Singh, C. Alvino, C. Bahlmann, and L. Grady, "Evaluating segmentation error without ground truth," in *International Conference on Medical Image Computing and Computer-Assisted Intervention*. Springer, 2012, pp. 528–536.
- [15] J. Fournel et al., "Medical image segmentation automatic quality control: A multi-dimensional approach," Medical Image Analysis, vol. 74, p. 102213, 2021.
- [16] W. Fan and I. Davidson, "Reverse testing: an efficient framework to select amongst classifiers under sample selection bias," in *Proceedings* of the 12th ACM SIGKDD international conference on Knowledge discovery and data mining, 2006, pp. 147–156.

- [17] E. Zhong et al., "Cross validation framework to choose amongst models and datasets for transfer learning," in Machine Learning and Knowledge Discovery in Databases: European Conference, ECML PKDD 2010, Barcelona, Spain, September 20-24, 2010, Proceedings, Part III 21. Springer, 2010, pp. 547–562.
- [18] N. Gaggion et al., "Chexmask: a large-scale dataset of anatomical segmentation masks for multi-center chest x-ray images," Scientific Data, vol. 11, no. 1, 2024.
- [19] R. Robinson et al., "Automatic quality control of cardiac mri segmentation in large-scale population imaging," in MICCAI 2017. Springer, 2017, pp. 720–727.
- [20] ——, "Real-time prediction of segmentation quality," in MICCAI 2018. Springer, 2018, pp. 578–585.
- [21] C. Ouyang, C. Biffi, C. Chen, T. Kart, H. Qiu, and D. Rueckert, "Self-supervised learning for few-shot medical image segmentation," *IEEE Transactions on Medical Imaging*, vol. 41, no. 7, pp. 1837–1848, 2022.
- [22] J. Snell, K. Swersky, and R. Zemel, "Prototypical networks for few-shot learning," in *Proceedings of the 31st International Conference on Neural Information Processing Systems*. Curran Associates Inc., 2017, p. 4080–4090.
- [23] C. Ouyang, C. Biffi, C. Chen, T. Kart, H. Qiu, and D. Rueckert, "Self-supervision with superpixels: Training few-shot medical image segmentation without annotation," in Computer Vision–ECCV 2020: 16th European Conference, Glasgow, UK, August 23–28, 2020, Proceedings, Part XXIX 16. Springer, 2020, pp. 762–780.
- [24] N. Ravi et al., "SAM 2: Segment anything in images and videos," in The Thirteenth International Conference on Learning Representations, 2025
- [25] Y. Bai, Q. Yu, B. Yun, D. Jin, Y. Xia, and Y. Wang, "Fs-medsam2: Exploring the potential of sam2 for few-shot medical image segmentation without fine-tuning." *CoRR*, vol. abs/2409.04298, 2024.
- [26] A. M. Wundram, P. Fischer, M. Mühlebach, L. M. Koch, and C. F. Baumgartner, "Conformal performance range prediction for segmentation output quality control," in *Uncertainty for Safe Utilization of Machine Learning in Medical Imaging*. Springer Nature Switzerland, 2025, pp. 81–91.
- [27] S. Kohl et al., "A probabilistic u-net for segmentation of ambiguous images," in Advances in Neural Information Processing Systems, vol. 31. Curran Associates, Inc., 2018.
- [28] C. F. Baumgartner et al., "Phiseg: Capturing uncertainty in medical image segmentation," in Medical Image Computing and Computer Assisted Intervention – MICCAI 2019: 22nd International Conference, Shenzhen, China, October 13–17, 2019, Proceedings, Part II. Springer-Verlag, 2019, p. 119–127.
- [29] M. S. Ayhan and P. Berens, "Test-time data augmentation for estimation of heteroscedastic aleatoric uncertainty in deep neural networks," in Medical Imaging with Deep Learning, 2018.
- [30] Y. Gal and Z. Ghahramani, "Dropout as a bayesian approximation: Representing model uncertainty in deep learning," in *Proceedings of The* 33rd International Conference on Machine Learning, vol. 48. PMLR, 2016, pp. 1050–1059.
- [31] B. Lakshminarayanan, A. Pritzel, and C. Blundell, "Simple and scalable predictive uncertainty estimation using deep ensembles," in *Advances in Neural Information Processing Systems*, vol. 30. Curran Associates, Inc., 2017.
- [32] Z. Li, K. Kamnitsas, M. Islam, C. Chen, and B. Glocker, "Estimating model performance under domain shifts with class-specific confidence scores," in *Medical Image Computing and Computer Assisted Inter*vention – MICCAI 2022: 25th International Conference, Singapore, September 18–22, 2022, Proceedings, Part VII. Springer-Verlag, 2022, p. 693–703.
- [33] P. Köhler, J. Fadugba, P. Berens, and L. M. Koch, "Efficiently correcting patch-based segmentation errors to control image-level performance in retinal images," in *Proceedings of The 7nd International Conference on Medical Imaging with Deep Learning*, vol. 250. PMLR, 2024, pp. 841–856.
- [34] C. Guo, G. Pleiss, Y. Sun, and K. Q. Weinberger, "On calibration of modern neural networks," in *Proceedings of the 34th International Conference on Machine Learning - Volume 70*. JMLR.org, 2017, p. 1321–1330.
- [35] L. Dabah and T. Tirer, "On temperature scaling and conformal prediction of deep classifiers," in Forty-second International Conference on Machine Learning, 2025.
- [36] A. Kirillov et al., "Segment anything," in Proceedings of the IEEE/CVF International Conference on Computer Vision (ICCV), 2023, pp. 4015– 4026

- [37] M. Oquab et al., "Dinov2: Learning robust visual features without supervision," 2024.
- [38] M. Douze et al., "The faiss library," 2024.
- [39] L. Zhao et al., "Retrieval-augmented few-shot medical image segmentation with foundation models," 2024.
- [40] F. Pérez-García et al., "Rad-dino: Exploring scalable medical image encoders beyond text supervision," 2024.
- [41] J. Lei, M. G'Sell, A. Rinaldo, R. J. Tibshirani, and L. Wasserman, "Distribution-free predictive inference for regression," 2017.
- [42] P. Radau, Y. Lu, K. Connelly, G. Paul, A. Dick, and G. Wright, "Evaluation framework for algorithms segmenting short axis cardiac mri," *The MIDAS Journal*, 2009.
- [43] T. L. van den Heuvel et al., "Automated measurement of fetal head circumference using 2d ultrasound images," PloS one, vol. 13, no. 8, p. e0200412, 2018.
- [44] J. Bai et al., "Psfhs challenge report: Pubic symphysis and fetal head segmentation from intrapartum ultrasound images," 2024.
- [45] T. Mendonca et al., "PH² a dermoscopic image database for research and benchmarking," in 2013 35th Annual International Conference of the IEEE Engineering in Medicine and Biology Society (EMBC). IEEE, 2013, pp. 5437–5440.
- [46] N. Codella et al., "Skin lesion analysis toward melanoma detection 2018: A challenge hosted by the international skin imaging collaboration (isic)," arXiv preprint arXiv:1902.03368, 2019.
- [47] M. Amgad et al., "Nucls: A scalable crowdsourcing approach and dataset for nucleus classification and segmentation in breast cancer," GigaScience, vol. 11, p. giac037, 2022.
- [48] J. Shiraishi et al., "Development of a digital image database for chest radiographs with and without a lung nodule: receiver operating characteristic analysis of radiologists' detection of pulmonary nodules," American journal of roentgenology, vol. 174, no. 1, pp. 71–74, 2000.
- [49] L. Soler et al., "3d image reconstruction for comparison of algorithm database: A patient specific anatomical and medical image database," IRCAD, Strasbourg, France, Tech. Rep, vol. 1, no. 1, 2010.
- [50] X. Zheng et al., "Fast and robust segmentation of white blood cell images by self-supervised learning," Micron, vol. 107, pp. 55–71, 2018.
- [51] O. Ronneberger, P. Fischer, and T. Brox, "U-net: Convolutional networks for biomedical image segmentation," in *Medical Image Computing and Computer-Assisted Intervention – MICCAI 2015*. Springer International Publishing, 2015, pp. 234–241.

APPENDIX A: CONTROLLED EXPERIMENTS ON EXCHANGEABILITY ASSUMPTION

To illustrate how exchangeability underpins Conformal RCA's coverage guarantees, we run a controlled experiment in which both calibration and test Dice scores are drawn from the same underlying distribution. RCA scores are then obtained by adding Gaussian noise to these true scores (clipped to [0,1]). We then apply Conformal RCA with the same settings used in Section V-C: a reference set of size 32 and empirical quantiles at levels $p_{\ell}=0.4$ and $p_h=0.95$.

Fig. 6 shows the resulting nonconformity-score histograms for calibration and test splits, along with the computed threshold \hat{q} . Empirical marginal coverage surpasses the desired 90 % target level, confirming that Conformal RCA achieves valid coverage under ideal conditions.

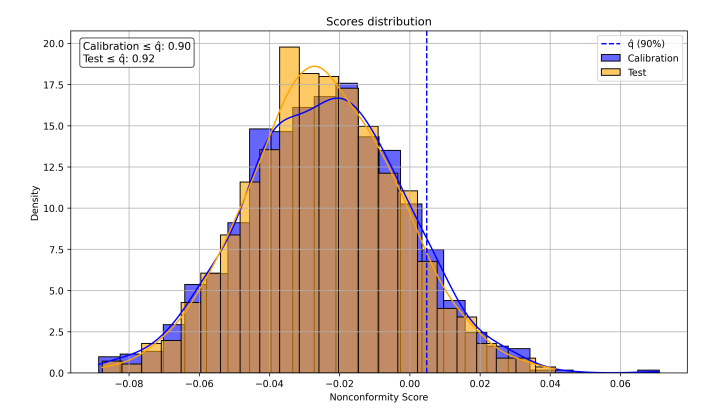


Fig. 6. Distribution of nonconformity scores for synthetic calibration and test sets, generated by sampling true Dice scores from a $\mathrm{Beta}(2,2)$ distribution and adding noise drawn from $\mathcal{N}(0,0.1)$ to simulate variability in RCA scores. The vertical dashed line indicates the conformal quantile threshold \hat{q} .